JOURNAL OF CATALYSIS **174,** 22–33 (1998)
ARTICLE NO. CA971944

Effects of Support Interaction on the Phase Stability of Rh Oxides Formed during the Aging of α-Alumina Supported Rh in Air

Zara Weng-Sieh,* Ronald Gronsky,* and Alexis T. Bell†

*Department of Materials Science and Mineral Engineering, University of California Berkeley, Berkeley, California 94720, and Materials Sciences Division, Lawrence Berkeley National Laboratory, Berkeley, California 94720; and †Department of Chemical Engineering, University of California Berkeley, Berkeley, California 94720, and Chemical Sciences Division, Lawrence Berkeley National Laboratory Berkeley, California 94720

Received May 16, 1997; revised September 30, 1997; accepted October 17, 1997

The phase stability of rhodium oxides formed during the aging of model α-alumina supported rhodium in air at temperatures of 500, 850, and 1000°C is investigated using high resolution transmission electron microscopy. The observed phases of rhodium oxides are similar to those predicted by bulk thermodynamics, with the RhO_2 phase formed at 500°C and the orthorhombic III-Rh_2O_3 phase formed at 1000°C. However, in some instances, the epitaxy of the rhodium oxide particles with the underlying α-alumina support appears to influence the phases formed, causing the presence of the hexagonal I-Rh_2O_3 phase at 500 and 850°C. Epitaxial stabilization of rhodium oxide phases is examined from the perspective of lattice matching at the oxide–support interface and minimization of the total oxide particle free energy.

INTRODUCTION

Rhodium is a key component of current three-way automotive emissions control catalysts and is used primarily to catalyze the reduction of NO (1). To maintain a high dispersion, Rh is supported on γ-alumina. Increasing requirements on the performance and durability of automotive converters (2) have stimulated an interest in understanding the microstructural changes occurring during the aging and deactivation of γ-alumina supported Rh (1). Aging in air below 650°C results in the formation of highly dispersed rhodium oxide moieties (3–5), recently identified as two dimension rafts of RhO_2 (6), and upon prolonged heating, small particles of RhO_2 and orthorhombic Rh_2O_3 (4–6). Above 650°C, large particles of orthorhombic Rh_2O_3 are observed (4–6), together with smaller particles of RhO_2 (6). Recent studies conducted with Rh supported on α-alumina have demonstrated that superior thermal stability can be achieved relative to what is observed using γ-alumina as the support (3, 7, 8). For example, significant loss in catalytic activity of α-alumina supported Rh occurs upon aging above 900°C, whereas the onset of loss in catalytic activity of γ-alumina supported Rh occurs upon aging above 650°C (3, 8). The superior thermal stability of α-alumina supported Rh has been attributed to factors such as the weaker interaction of the Rh on the α-alumina support (3) and the ability to maintain higher dispersion of Rh on α-alumina (7). However, the nature of the rhodium oxides formed during aging in air is still unclear. Most recently, XPS results reported by Lakis *et al.* (9) suggest the presence of mixed oxide states for Rh, after calcination of Pt-Rh/γ-alumina at 500°C followed by reduction at 300°C. It is important to note that within these aging temperatures (500–1050°C), there are several known thermodynamically stable bulk rhodium oxide phases (10–16).

An interesting finding of thermal aging studies has been the observation that the phase of rhodium oxide observed after aging at a given temperature does not necessarily coincide with that expected on the basis of bulk-phase thermodynamics. For example, orthorhombic Rh_2O_3 is observed at 500°C (4, 5), whereas bulk-phase thermodynamics predicts that only tetragonal RhO_2 should be stable (10–16). Likewise, particles of RhO_2 are observed following aging at 1000°C (6) where orthorhombic Rh_2O_3 particles are expected on the basis of bulk-phase thermodynamics (10–16). While it has been suggested that interactions between the alumina support and the particles of rhodium oxide may contribute to the stabilization of unexpected rhodium oxide phases (6), confirmation of this interpretation has been encumbered by the concurrent phase transformation of γ-alumina during thermal aging. For this reason, we have undertaken an investigation of the thermal aging of Rh supported on α-alumina. The goal of this work is to identify the role of the support in stabilizing phases of rhodium oxide different from those anticipated from bulk-phase thermodynamics and in particular to establish the extent to which oxide–support epitaxy and the size of the dispersed oxide particles affect the stabilization of rhodium oxide phases. The work is conducted with a sample of 15% Rh/α-alumina aged in air at temperatures of 500, 850, and 1000°C. Microstructural characterization of the rhodium

0021-9517/98 $25.00

TABLE 1

Crystallographic Data of Known Rh Oxides

Composition	Structure	a_0 (Å)	b_0 (Å)	c_0 (Å)	Space group	Ref.
Rh_2O_3-I	Hexagonal	5.13	—	13.85	*R*-3*c*	11
Rh_2O_3-II	Orthorhombic	5.14	5.44	14.69	*Pbca*	12
Rh_2O_3-III	Orthorhombic	5.17	5.38	7.24	*Pbna*	13
RhO_2	Tetragonal	4.49	—	3.09	*P*42/*mnm*	14

oxide particles is done exclusively by high resolution transmission electron microscopy (HRTEM) because of the superior spatial resolution it affords, as needed for detailed assessment of small particle and interfacial characteristics.

EXPERIMENTAL

Alpha-alumina supported rhodium (15 wt.%) is prepared by incipient wetness impregnation of dried α-alumina (Meller Optics, 2 m^2/g) with an aqueous solution of rhodium(III) trichlorohydrate ($RhCl_3 \cdot 3H_2O$) (Johnson-Matthey). The catalyst is then dried at 120°C for 2 h, calcined in air flowing at 100 cm^3/min at 400°C for 4 h, and reduced in H_2 at 400°C for 4 h. The reduced catalyst is then passivated by exposure to 1000 ppm O_2/He at room temperature for 20 min. Samples of the catalyst are aged in air for 71 h at 500°C, for 50 h at 850°C, and for 5 h at 1000°C.

TEM specimens are prepared by crushing the catalyst between two glass slides and dry-dispersing the catalyst onto a holey-carbon covered TEM grid. HRTEM is performed on a Topcon 002B electron microscope operating at 200 kV, with a nominal point-to-point resolution of 1.9 Å. Rhodium oxide phases are identified by Fourier analysis of HRTEM images, from which precise determination of lattice spacings and interplanar angles can be made. Table 1 shows a summary of the crystallographic data for the known phases of rhodium oxide (10–16). HRTEM images are also used to characterize the interface between the rhodium oxide particles and the α-alumina support. The interfaces are classified into one of three different types: coherent, semicoherent, and incoherent (17). Fully coherent interfaces are observed when two lattices are continuous across the interface. To fulfill this requirement, both phases must be oriented such that their interatomic spacings and configurations are perfectly matched across the interface. When the interatomic spacings differ, coherency across the interface can be maintained by straining one or both lattices. The effective lattice misfit across the interface is defined by $d = (a_2 - a_1)/a_1$ where a_1 and a_2 are the lattice *parameters* of the unstrained lattices of the support (a_1) and the particle (a_2). When the lattice misfit increases ($0 < d < 0.25$), it becomes energetically favorable to form semicoherent interfaces in which misfit dislocations are formed across an interface to relieve the coherency strains. These misfit dislocations that relieve coherency strains comprise a series of dislocations with equilibrium spacing, D, given by $D = a_1/d$, for $a_2 > a_1$. In cases of poor matching across the interface ($d > 0.25$), an incoherent interface may be formed.

RESULTS

After samples were aged for 71 h at 500° C, HRTEM images reveal particles of both tetragonal RhO_2 and hexagonal I-Rh_2O_3 that exhibit epitaxy with the underlying α-alumina support. Figure 1a shows two RhO_2 particles. The particle on the left has a diameter of 69 Å and the

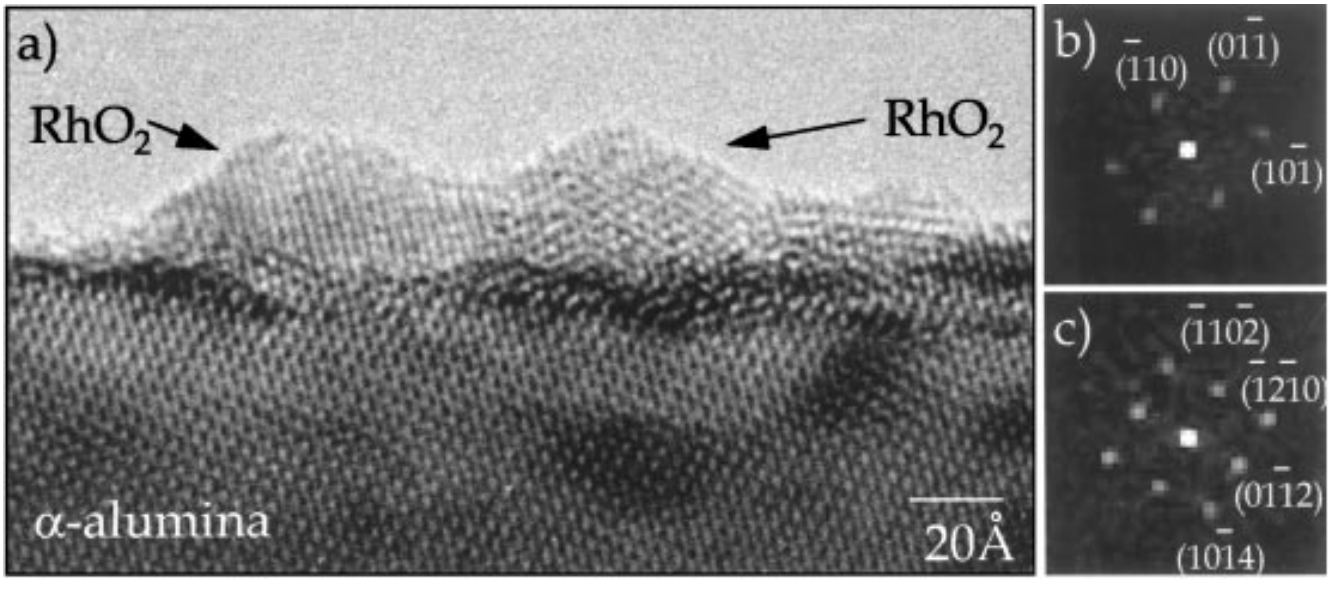

FIG. 1. (a) HRTEM image of RhO_2 particle formed after aging 71 h at 500°C; (b) diffractogram of particle, indicating the [111] orientation of the RhO_2 structure; (c) diffractogram of support, revealing the [2021] orientation.

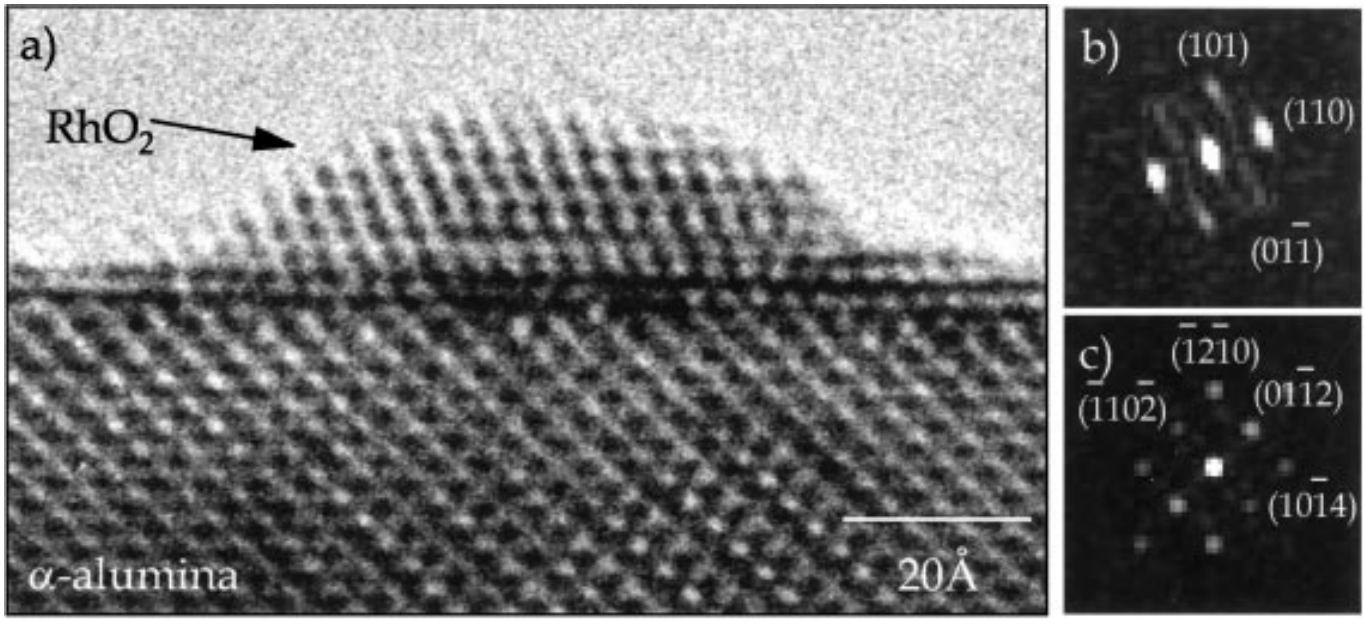

FIG. 2. (a) HRTEM image of RhO_2 particle formed after aging 71 h at 500°C; (b) diffractogram of particle, indicating the [$\bar{1}$11] orientation of the RhO_2 structure; (c) diffractogram of support, revealing the [20$\bar{2}$1] orientation.

one on the right has a diameter of 58 Å. Both particles are about 24 Å high. The diffractogram of the rhodium oxide particle on the right (Fig. 1b) reveals reflections corresponding to the (10$\bar{1}$)and (01$\bar{1}$) planes, which are characteristic of the RhO_2 phase, as viewed along its [11$\bar{1}$] zone axis. The measured angle between the (10$\bar{1}$) and (01$\bar{1}$) planes is 46.7°, which is close to the calculated angle of 47.3°. The α-alumina support is viewed along its [20$\bar{2}$1] zone axis, and the diffractogram (Fig. 1c) of the α-alumina support reveals reflections corresponding to the (01$\bar{1}$2) and (1$\bar{1}$02) α-alumina planes, which have interplanar spacings of 3.48 Å. The measured angle between the (01$\bar{1}$2) and (1$\bar{1}$02) planes is 93.9°, which is close to the calculated angle of 94.0°. The (12$\bar{1}$0) planes of the α-alumina support and the (01$\bar{1}$) planes of the RhO_2 particle are parallel, indicating epitaxy of the RhO_2 particles on the support. The (12$\bar{1}$0) α-alumina (01$\bar{1}$) and RhO_2 planes have interplanar spacings of 2.38 and 2.55 Å, respectively, and the mismatch between these planes, given by $(d_{RhO_2} - d_{Al_2O_3}/d_{Al_2O_3})$, is 7.1%. However, since the (12$\bar{1}$0) α-alumina and (01$\bar{1}$) RhO_2 planes occur at an angle of approximately 15° from the interface normal, the effective lattice mismatch between the heterostructures, given by the difference in parallel interplanar spacings of the individual phases that occur normal to the interface, is approximately 7.4%. The observation of periodic strain fields at the particle-support interface, separated by approximately 70 Å intervals, indicates the presence of misfit dislocations. These dislocations relieve the coherency strains associated with the large lattice mismatch, causing the formation of a semicoherent interface between the particle and support. This lattice mismatch is also partially accommodated by a compressive strain in the rhodium oxide particle, which causes a slight contraction of the (01$\bar{1}$) RhO_2 planes such that the interplanar spacings decrease from 2.55 Å (bulk) to 2.52 Å (measured).

A RhO_2 particle that forms a different interface with the alumina support is displayed in Fig. 2a. This particle is approximately 73 Å in diameter and 18 Å high. The diffractogram of the rhodium oxide particle (Fig. 2b) reveals reflections corresponding to the (101) and (110) planes, which are characteristic of the RhO_2 phase, as viewed along its [$\bar{1}$11] zone axis. The measured angle between the (101) and (110) planes is 68.5°, which is close to the calculated angle of 66.0°. The α-alumina support is viewed along its [(20$\bar{2}$1)] zone axis, and the diffractogram (Fig. 2c) of the α-alumina support reveals reflections corresponding to the (01$\bar{1}$2) and (1$\bar{1}$02) α-alumina planes, which have interplanar spacings of 3.48 Å. The measured angle between the (01$\bar{1}$2) and (1$\bar{1}$02) planes is 92.7°, which is close to the calculated angle of 94.0°. In this case, the (1$\bar{1}$02) planes of the α-alumina support and the (01$\bar{1}$) planes of the RhO_2 phase occur in almost the same direction with a 10° rotation, but deviate from the [10$\bar{1}$1] interface direction. By using the orientation relationship $(01\bar{1})_{RhO_2}//(12\bar{1}0)_{Al_2O_3}$ and $[11\bar{1}]_{RhO_2}//[1\bar{1}01]_{Al_2O_3}$ determined from other RhO_2-α-alumina interfaces, it can be shown that normal to the [100] interface are the (12$\bar{2}$) RhO_2 planes and the (20$\bar{2}$8) α-alumina planes. Hence, the lattice misfit across the interface, given by the difference between the (12$\bar{2}$) RhO_2 planes with interplanar spacings of 1.22 Å and the (20$\bar{2}$8) α-alumina planes with interplanar spacings of 1.28 Å, is −4.7%. In this instance, the formation of an epitaxial interface between the RhO_2 particle and

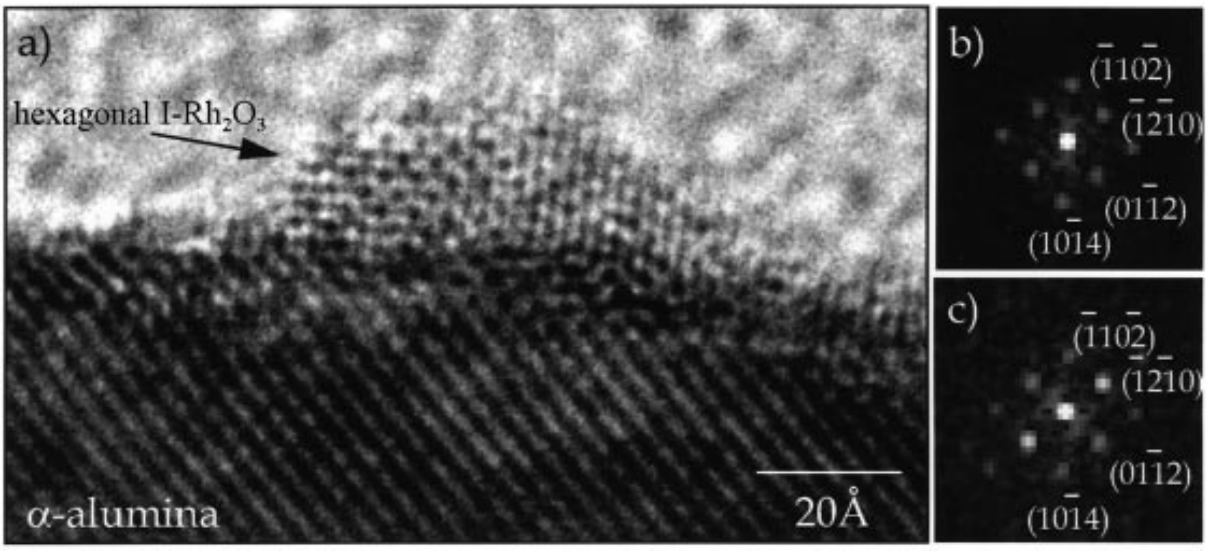

FIG. 3. (a) HRTEM image of hexagonal I-Rh_2O_3 particle formed after aging 71 h at 500°C; (b) diffractogram of particle, indicating the [20$\bar{2}$1] orientation of the hexagonal I-Rh_2O_3; (c) diffractogram of support, revealing the [20$\bar{2}$1] orientation.

the α-alumina support results in a smaller lattice mismatch across the interface.

A low temperature, low pressure (LT, LP) hexagonal I-Rh_2O_3 phase particle exhibiting a semicoherent interface with the underlying α-alumina support is shown in Fig. 3a. This particle, as viewed along its [20$\bar{2}$1] zone axis, is approximately 60 Å wide and 20 Å high. The diffractogram of the rhodium oxide particle shown in Fig. 3b reveals reflections corresponding to the (1$\bar{1}$02) and (01$\bar{1}$2) planes, which have interplanar spacings of 3.74 Å characteristic of the LT, LP hexagonal I-Rh_2O_3 phase. The measured angle between the (1$\bar{1}$02) and (01$\bar{1}$2) planes is 87.8°, which is close to the calculated angle of 86°. The diffractogram of the α-alumina support shown in Fig. 3c illustrates the [20$\bar{2}$1] zone axis with reflections corresponding to the (1$\bar{1}$02) and (01$\bar{1}$2) α-alumina planes, which have interplanar spacings of 3.48 Å. As indicated by the HRTEM image and the diffractogram, the (1$\bar{1}$02) planes originating from the α-alumina and the hexagonal Rh_2O_3 particle occur in the same orientations, indicating an epitaxial relationship between the rhodium oxide and the α-alumina support. The lattice misfit between the (1$\bar{2}$10) α-alumina and (1$\bar{2}$10) hexagonal I-Rh_2O_3 planes, which have interplanar spacings of 2.38 and 2.56 Å, respectively, is 7.6%. In this case, both the hexagonal I-Rh_2O_3 particle and the hexagonal α-Al_2O_3 support are observed in the same orientation, obeying the orientation relationship $(10\bar{1}0)_{Rh_2O_3}//(10\bar{1}0)_{Al_2O_3}$ and $[0001]_{Rh_2O_3}//[0001]_{Al_2O_3}$.

HRTEM images indicate that after aging for 50 h at 850°C large Rh_2O_3 particles are formed, exhibiting substantial interfacial contact with the support. Figure 4a reveals an example of such a particle, which is 75 Å in diameter and 30 Å high, as viewed along its [$\bar{1}$10$\bar{1}$] zone axis. The diffractogram of the rhodium oxide particle (Fig. 4b) reveals reflections corresponding to the (02$\bar{2}\bar{2}$) and (20$\bar{2}$2) planes, which have interplanar spacings of 1.96 Å, characteristic of the LT, LP hexagonal I-Rh_2O_3. The measured angle between the (02$\bar{2}\bar{2}$) and (20$\bar{2}$2) planes is 69.0°, which is close to the calculated angle of 68.7°. The diffractogram (Fig. 4c) of the α-alumina support reveals reflections corresponding to the (02$\bar{2}\bar{2}$) and (2022) α-alumina planes, as viewed along the same orientation, the [$\bar{1}$10$\bar{1}$] zone axis. The 1.74 Å lattice spacings originating from the (2$\bar{2}$04) planes of α-alumina and the 1.86 Å fringes originating from the (2$\bar{2}$04) planes of Rh_2O_3 occur in the same direction, from which it is deduced that $(10\bar{1}0)_{Rh_2O_3}//(10\bar{1}0)_{Al_2O_3}$ and $[0001]_{Rh_2O_3}//[0001]_{Al_2O_3}$. The effective lattice misfit in this case is 7.4%. As seen in Fig. 4a, the Rh_2O_3 particle forms interfaces with the α-alumina support along three of the particle edges, suggesting that the formation of the interfaces leads to a decrease in the surface free energy in spite of the strain energy associated with lattice misfit across the interface.

Figure 5a shows another hexagonal I-Rh_2O_3 particle which is 105 Å in diameter and 35 Å high, viewed along its [1101] zone axis. The diffractogram of the rhodium oxide particle (Fig. 5b) exhibits reflections corresponding to the (02$\bar{2}\bar{2}$) and (20$\bar{2}$2) planes, which have interplanar spacings of 2.11 Å and are characteristic of hexagonal I-Rh_2O_3. The measured angle between the (02$\bar{2}\bar{2}$) and (20$\bar{2}$2) planes is 67.5°, which is close to the calculated angle of 68.7°. The diffractogram of the α-alumina support shown in Fig. 5c reveals reflections corresponding to the (02$\bar{2}\bar{2}$) and (20$\bar{2}$2) α-alumina planes, as viewed along its (1$\bar{1}$01) zone axis. This particle exhibits the same epitaxial relationship with the

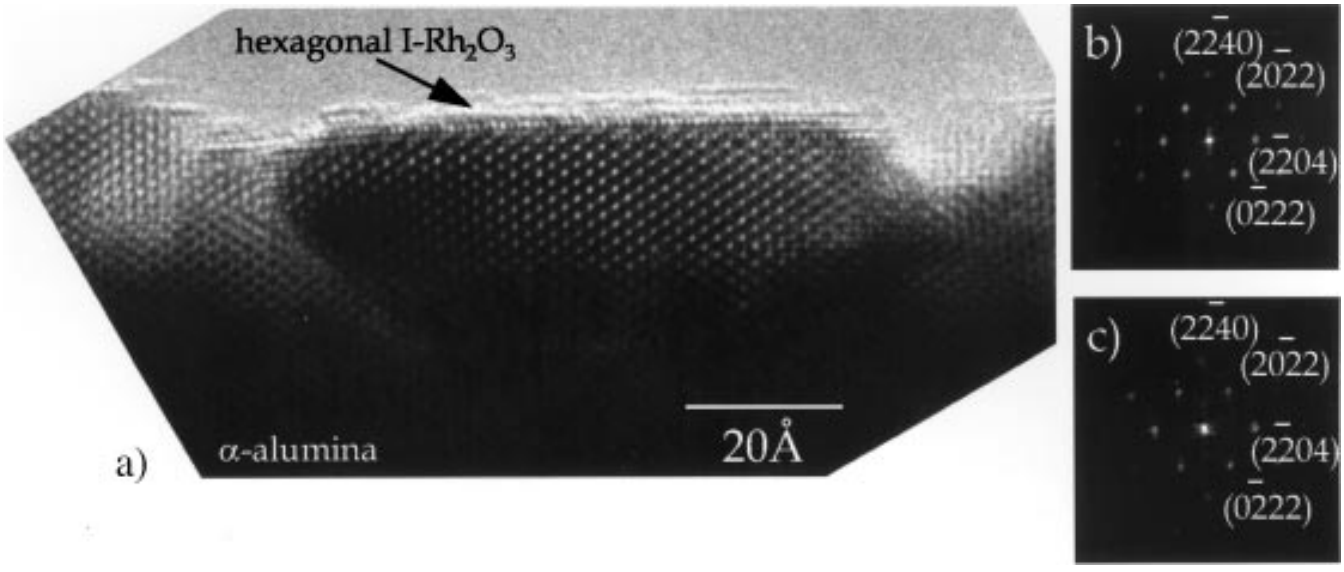

FIG. 4. (a) HRTEM image of hexagonal I-Rh_2O_3 particle formed after aging 50 h at 850°C; (b) diffractogram of particle, indicating the $[\bar{1}10\bar{1}]$ orientation of the hexagonal I-Rh_2O_3 structure; (c) diffractogram of support, revealing the $[\bar{1}10\bar{1}]$ orientation.

support observed for the hexagonal I-Rh_2O_3 particle shown in Fig. 4.

After aging for 5 h at 1000°C, both the high temperature, high pressure (II) and high temperature, low pressure (III) orthorhombic Rh_2O_3 phases are observed. In many instances, the rhodium oxide-alumina interface is semicoherent, as evidenced by the presence of misfit dislocations. Figure 6a shows a particle of HT, LP (III) orthorhombic Rh_2O_3 which is 260 Å in diameter and 143 Å high. The diffractogram of the image (Fig. 6b) reveals reflections corresponding to the (020) HT, LP Rh_2O_3 planes, which have interplanar spacings of 2.72 Å, and the $(10\bar{1}4)$ α-Al_2O_3 planes, which have interplanar spacings of 2.55 Å. In this case, the 2.55 Å lattice spacings originating from the $(10\bar{1}4)$ planes of α-alumina and the 2.72 Å fringes originating from the (020) planes of HT, LP III-Rh_2O_3 are parallel, indicating the formation of an epitaxial interface. The effective lattice misfit across the interface is 6.7%. The lattice

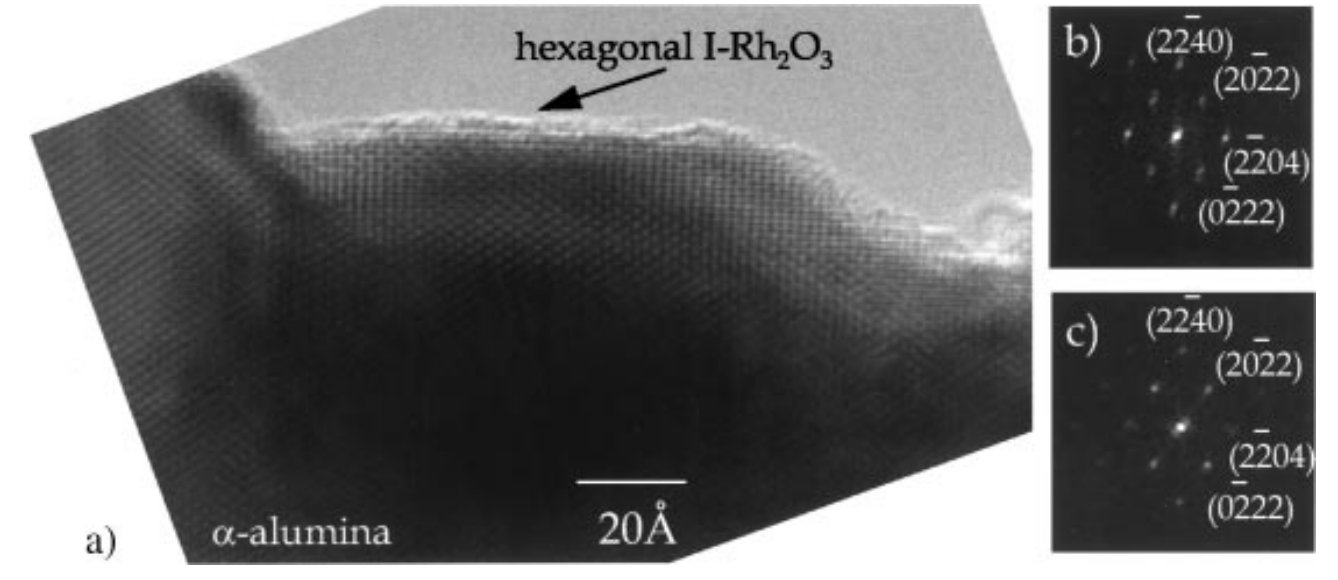

FIG. 5. (a) HRTEM image of hexagonal I-Rh_2O_3 particle formed after aging 50 h at 850°C; (b) diffractogram of particle, indicating the $[\bar{1}10\bar{1}]$ orientation of the hexagonal I-Rh_2O_3 structure; (c) diffractogram of support, revealing the $[\bar{1}10\bar{1}]$ orientation.

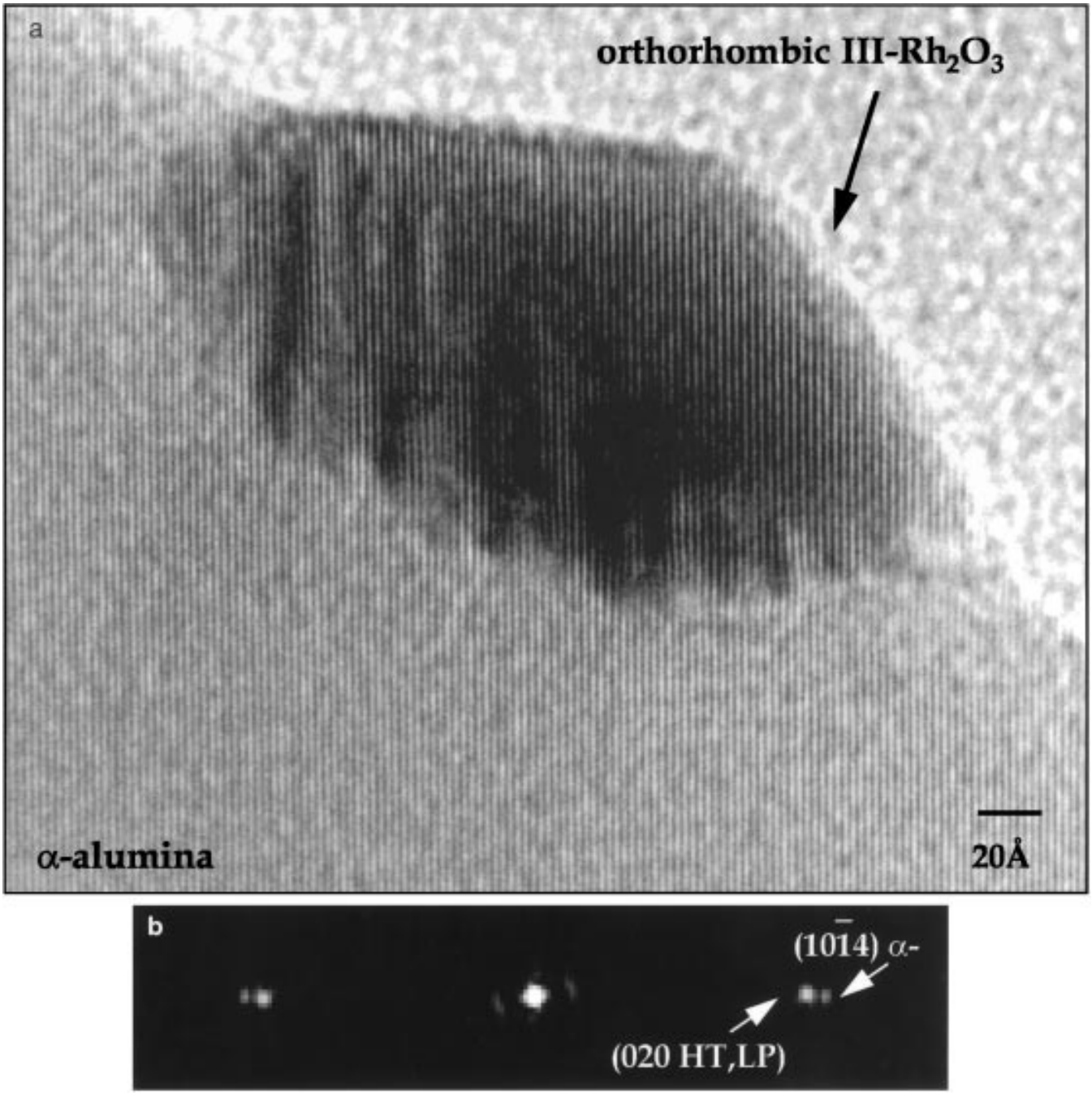

FIG. 6. (a) Lattice image of HT, LP orthorhombic III-Rh_2O_3 particle formed after aging 5 h at 1000°C; (b) diffractogram of particle and support, revealing the (020) orthorhombic III-Rh_2O_3 reflections and the (10$\bar{1}$4) reflections.

mismatch across this interface is accommodated by a regular series of misfit dislocations.

Figure 7a shows an orthorhombic HT, HP II-Rh_2O_3 particle which is 160 Å in diameter and 80 Å high. The diffractogram of the image (Fig. 7b) reveals reflections corresponding to the (021) HT, HP II-Rh_2O_3 planes, which have interplanar spacings of 2.52 Å, and the (11$\bar{2}$0) α-Al_2O_3 planes, which have interplanar spacings of 2.38 Å. In this case, the 2.38 Å lattice spacings originating from the (11$\bar{2}$0) α-alumina support and the 2.52 Å fringes originating from the (021) HT, HP II-Rh_2O_3 phase are parallel, again indicating the formation of an epitaxial interface. The lattice misfit across the interface is 5.9%. This lattice mismatch across the interface is accommodated by irregularly spaced misfit dislocations, identified by the white arrows.

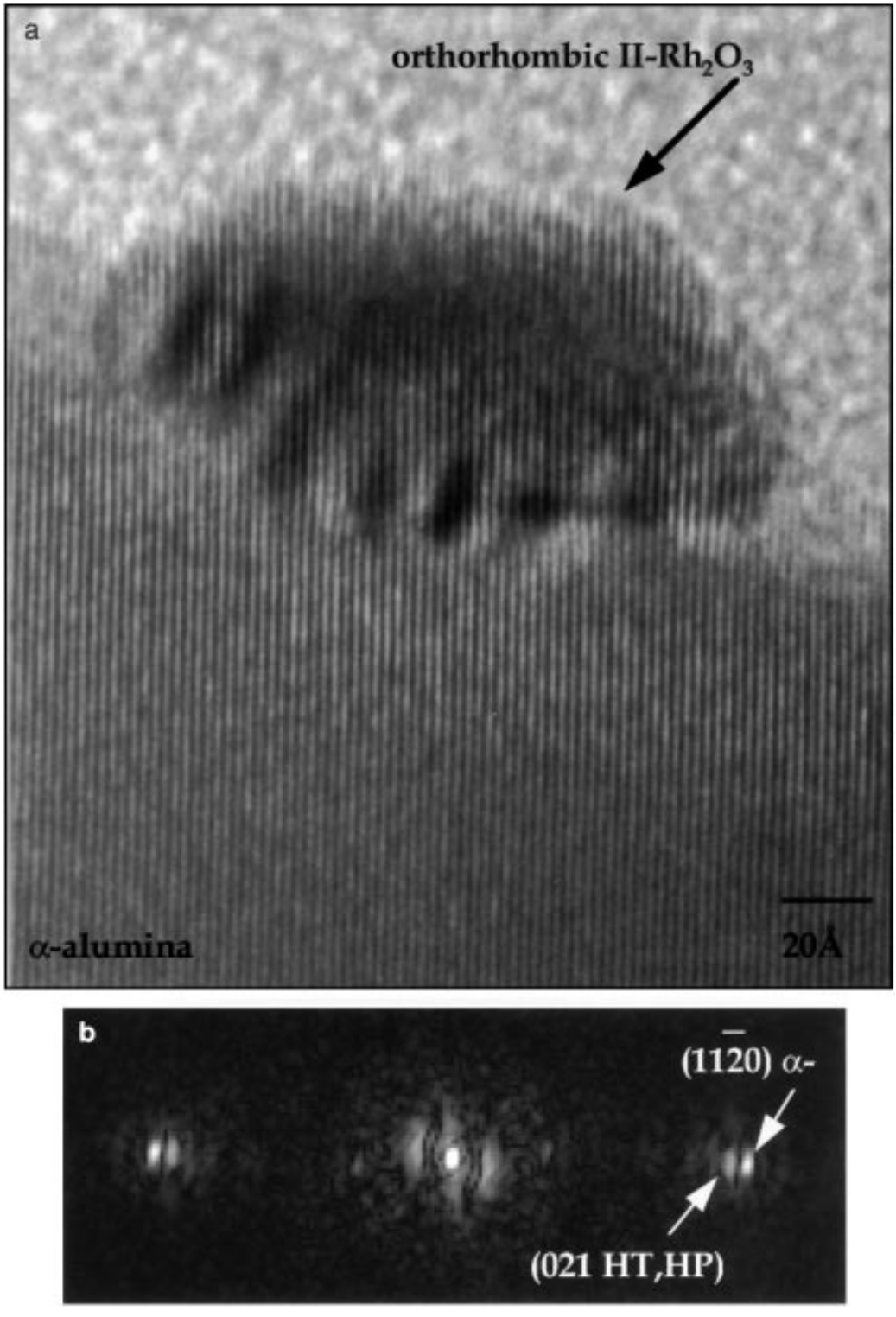

FIG. 7. (a) Lattice image of HT, HP orthorhombic II-Rh_2O_3 particle formed after aging 5 h at 1000°C; (b) diffractogram of particle and support, revealing the (021) orthorhombic II-Rh_2O_3 reflections and the $(1\bar{1}20)$ reflections.

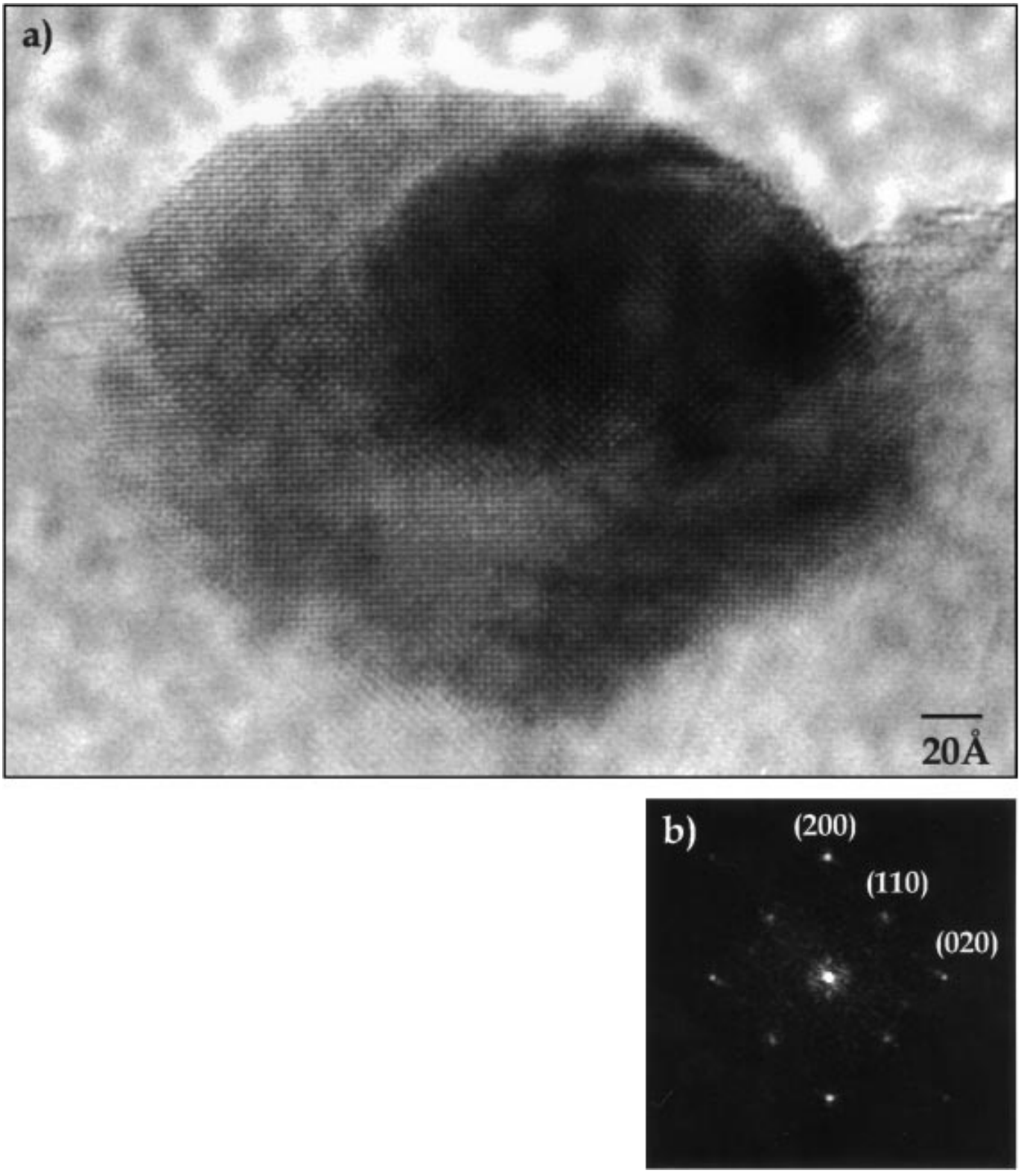

FIG. 8. (a) HRTEM image of HT, HP orthorhombic II-Rh_2O_3 particle formed after aging 5 h at 1000°C; (b) diffractogram of particle, indicating the [001] orientation.

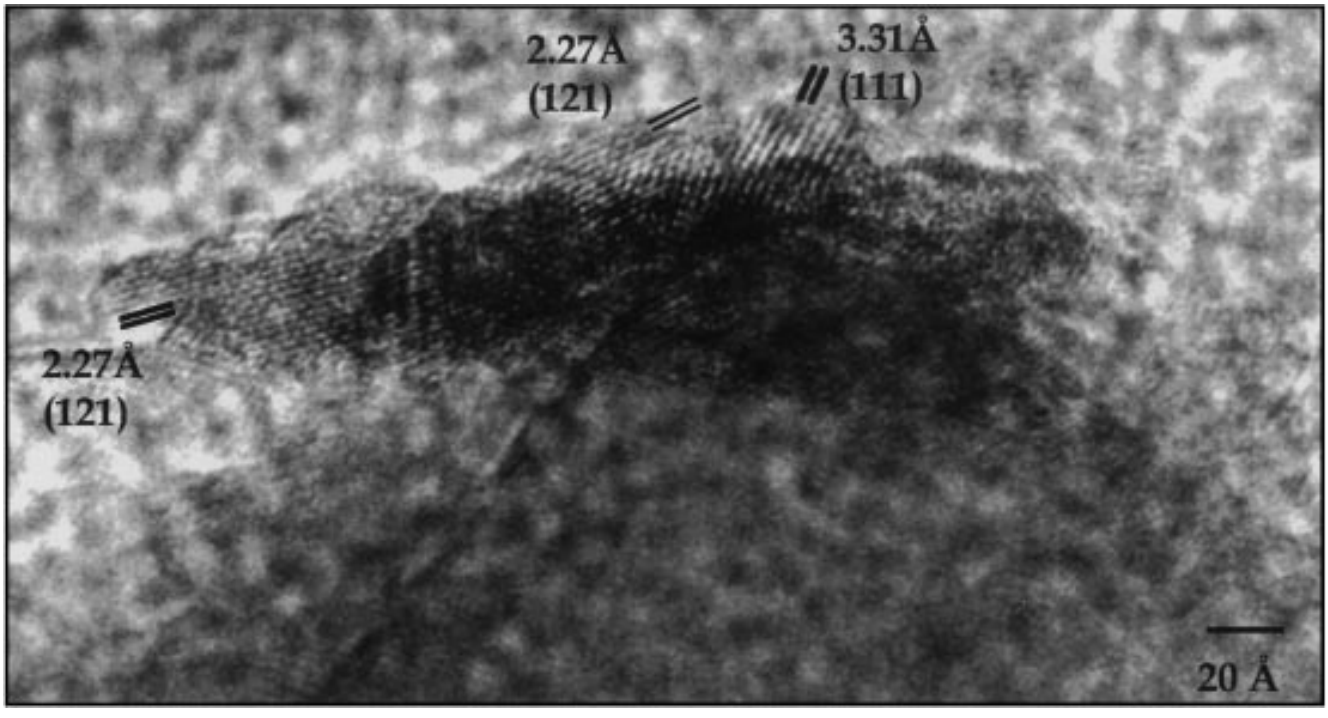

FIG. 9. HRTEM image of disordered HT, HP orthorhombic II-Rh_2O_3 particle formed after aging 5 h at 1000°C.

Aging at 1000°C not only results in the formation of the orthorhombic Rh_2O_3 polymorphs, but also causes interesting changes in the microstructure of the oxide particles. In several instances, the rhodium oxide particles straddle a grain boundary separating two alumina grains. An example of such a Rh_2O_3 particle is shown in Fig. 8a. This particle is 267 Å in diameter and 200 Å high. The diffractogram of the rhodium oxide particle (Fig. 8b) exhibits reflections corresponding to the (110) and ($\bar{1}$10) planes, which have interplanar spacings of 3.73 Å, characteristic of the HT, HP II-Rh_2O_3 phase. The measured angle between the (110) and ($\bar{1}$10) planes is 86.0°, which is close to the calculated angle of 88.4°. Structurally disordered rhodium oxide particles are also observed, as shown in Fig. 9. This HT, HP orthorhombic II-Rh_2O_3 particle is approximately 267 Å in diameter and 27 Å high. Several families of (111) and (121) planes are observed in this particle, indicating polycrystallinity.

DISCUSSION

The results of this study clearly show that many of the rhodium oxide particles formed upon aging of α-alumina supported rhodium exhibit epitaxy with the support. At low temperatures (e.g., 500°C), the oxide particles are small and the particle-support interfaces are either semicoherent or fully coherent. Higher aging temperatures (e.g., 850°C) result in the formation of larger oxide particles and a semicoherent interface, with misfit dislocations that relieve the interfacial strain arising from lattice mismatch across the interface. When aging occurs at very high temperatures (e.g., 1000°C) the particles of rhodium oxide grow further in size and the oxide-support interface becomes increasingly incoherent.

It is notable that the rhodium oxide phases observed at different aging temperatures are not fully consistent with those that would be expected from bulk thermodynamics. Based on the phase stability studies of Carol and Mann (15) and Muller and Roy (14), one would expect RhO_2 to be the thermodynamically favorable phase at 500°C and orthorhombic III-Rh_2O_3 to be the stable phase at 850 and 1000°C. Our HRTEM results indicate that both the tetragonal RhO_2 and hexagonal I-Rh_2O_3 phases are formed at 500°C, the hexagonal I-Rh_2O_3 phase is formed at 850°C, and the HT, HP (II) and HT, LP (III) Rh_2O_3 phases are formed at 1000°C. The observation of hexagonal I-Rh_2O_3 particles at 500 and 850°C on (10$\bar{1}$4) α-alumina surfaces and of tetragonal RhO_2 particles at 500°C on (1$\bar{2}$10) α-alumina surfaces suggests that the interface may be responsible for the stabilization of these phases.

The contribution of interfacial interactions to the thermodynamic stability of small metal oxide particles can be described (assuming a coherent interface and isotropy of the surface and interface free energy) in terms of

$$G = G_0 V + A_{\text{surf}}\gamma_{\text{surf}} + A_{\text{int}}\gamma_{\text{int}} - A_{\text{int}}\gamma_{\text{supp}}, \qquad [1]$$

where G_0 is the free energy per unit volume of the unstrained bulk phase; V is the volume of the particle; γ_{surf},

γ_{int}, and γ_{supp} are the free energy per unit area of the oxide-gas surface, the oxide-support interface, and the support-gas surface; and A_{surf} and A_{int} are the surface areas of the oxide-gas and oxide-support surfaces, respectively. G_0, γ_{supp}, and γ_{surf} depend solely on the properties of the bulk oxide phases, whereas γ_{int} depends on the properties of the bulk oxide phase and the oxide-support interactions. The interfacial free energy per unit area, γ_{int}, comprises two contributions, chemical bonding and strain:

$$\gamma_{int} = \gamma_{chem} + \gamma_{strain}. \quad [2]$$

The formation of chemical bonds between the oxide particles and the support will lower the value of γ_{int} whereas lattice strain will raise the value of γ_{int}. A close match between the interatomic spacings of the oxide particle and the support at the oxide-support interface should contribute to a reduction in the value of γ_{int} due to the formation of chemical bonds and the minimization of lattice strain.

In light of the preceding discussion, it is conceivable that for small oxide particles, interfacial interactions can reduce the overall free energy of the system, so that thermodynamically unfavorable bulk oxide phases are stabilized. The stabilization of such dimensionally restricted oxide phases would depend as well on the plane of the support being considered. The proposed epitaxial stabilization of metastable or competing bulk structures is known to occur for metals and semiconductor compounds (18–21). For example, Sands *et al.* (21) have observed the influence of substrate orientation on phase formation. Under the same processing conditions, on the hexagonal CdS substrate, the thermodynamically favored low pressure chalcocite Cu_2S is formed on surfaces inclined to the basal plane, while the high pressure tetragonal Cu_2S polymorph is formed on basal-plane oriented CdS surfaces (21).

As noted earlier, the $(10\bar{1}4)$ surface stabilizes hexagonal I-Rh_2O_3, whereas the (1210) surface of the α-Al_2O_3 stabilizes RhO_2. To understand why this occurs, it is useful to examine the possible arrangement of the atoms in both the oxide and the support at the oxide-support interface. As shown in Fig. 10, the $(10\bar{1}4)$ plane has a *pseudo-hexagonal* arrangement of oxygen atoms, separated by distances of 3.95 and 4.76 Å. It is evident from Fig. 10a that there is a good match between the oxygen atoms of the $(10\bar{1}4)$ α-Al_2O_3 plane and those of the$(10\bar{1}4)$ Rh_2O_3 plane, which has a pseudo-hexagonal arrangement of oxygen atoms, separated by distances of 4.19 and 5.15 Å. The closest orientational relationship that could be established between the $(10\bar{1}4)$ surface of α-Al_2O_3 and RhO_2 would be with the (100) surface of the latter oxide. As shown in Fig. 10b, the (100) RhO_2 and $(10\bar{1}4)$ α-alumina surfaces are very poorly matched, and hence, one would not expect the $(10\bar{1}4)$ surface of alumina to be conducive to the stabilization of RhO_2 particles. By contrast, Fig. 11a shows that the oxygen atoms

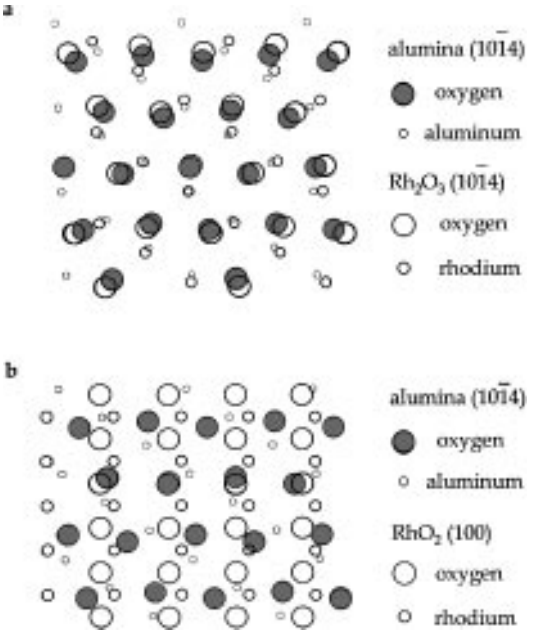

FIG. 10. Interfacial arrangement of oxygens for hexagonal I-Rh_2O_3-α-alumina interface shown in Fig. 3. (a) A good matching is observed upon overlaying the pseudo-hexagonal arrangement of oxygens for $(10\bar{1}4)$ hexagonal I-Rh_2O_3 on the $(10\bar{1}4)$ α-alumina. (b) A poor matching is observed upon overlaying the rectangular (100) RhO_2 arrangement of oxygens on the pseudo-hexagonal arrangement of oxygens for $(10\bar{1}4)$ α-alumina.

of the (101) surface of RhO_2 show good registry with oxygen atoms in the α-alumina surface. The $(12\bar{1}0)$ plane of α-alumina has a *pseudo-rectangular* arrangement of oxygen atoms that are separated by distances of 2.53–2.86 and 4.34 Å (Fig. 11a), whereas the (101) surface of RhO_2 has a pseudo-rectangular arrangement of oxygen atoms that are separated by distances of 2.77 and 4.49 Å (Fig. 11a). While Fig. 11b also suggests reasonably good registry between the oxygen atoms in the $(12\bar{1}0)$ surface of hexagonal I-Rh_2O_3 and the $(\bar{1}2\bar{1}0)$ surface of α-alumina, the degree of lattice matching is not as good as that between the $(10\bar{1}4)$ planes of I-Rh_2O_3 and $(10\bar{1}4)$ planes of α-alumina. The surface of the $(\bar{1}2\bar{1}0)$ I-Rh_2O_3 has a pseudo-rectangular arrangement of oxygen atoms that are separated by distances of 2.68–3.03 and 4.69 Å (Fig. 11b). Arguments similar to these can be used to explain the observation of hexagonal I-Rh_2O_3 after aging at 850°C, whereas orthorhombic III-Rh_2O_3 is the thermodynamically favored bulk phase.

It is interesting to note that the observed epitaxial relationships between RhO_2 and α-alumina, and hexagonal I-Rh_2O_3 and α-alumina, are not the most favored with respect to lattice misfit. For example, in the hexagonal I-Rh_2O_3-α-alumina system, it is observed (Fig. 4) that the $(2\bar{2}04)$ hexagonal I-Rh_2O_3 planes, which have interplanar spacings of 2.56 Å, are parallel to the $(2\bar{2}04)$ α-alumina planes, which have interplanar spacings of 1.74 Å,

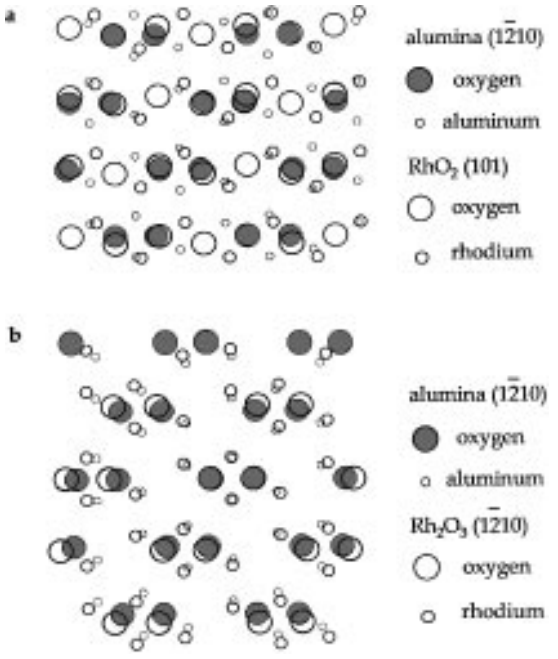

FIG. 11. Interfacial arrangement of oxygens for tetragonal RhO_2-α-alumina interface shown in Fig. 2. (a) A good matching is observed upon overlaying the pseudo-rectangular arrangement of oxygens for the (101) tetragonal RhO_2 on the pseudo-rectangular arrangement of oxygens for the (1$\bar{2}$10) α-alumina. (b) A slightly worse matching is observed upon overlaying the rectangular (1$\bar{2}$10) Rh_2O_3 arrangement of oxygens on the pseudo-rectangular arrangement of oxygens for (1$\bar{2}$10) α-alumina.

resulting in a large lattice misfit of 7.4%. A smaller lattice misfit of 1.1% would have been possible if the (11$\bar{2}$6) hexagonal I-Rh_2O_3 planes, which have interplanar spacings of 1.72 Å, were parallel to the (2$\bar{2}$04) α-alumina planes. It is conceivable that the latter arrangement of planes is not observed because it would lead to a higher contribution to $A_{surf}\ \gamma_{surf}$, while lowering the value of $A_{int}\ \gamma_{int}$ in Eq. [1]. This suggests that thermodynamic control of rhodium oxide microstructure forces rhodium oxide particles to assume structures that minimize the total free energy of the particle.

The absence of fully coherent interfaces between rhodium oxide and α-alumina at higher temperatures is attributable to two factors. The first is the smaller ratio of interfacial surface area to particle volume and the second is the enhanced rate of forming misfit dislocations due to the higher aging temperature. Both factors contribute to a reduction in the contribution of the interfacial free energy to the total free energy of the particle (see Eq. [1]). For very large particles, the effects of interfacial free energy become insignificant and the distribution of oxide phases is now dominated by bulk thermodynamics.

Based on the present discussion, it is expected that the nature of the rhodium oxide phases that could be stabilized on other phases of alumina would differ from those observed for α-alumina. This might explain why in an earlier aging study conducted with γ-alumina supported rhodium (6), we reported the observation of both the orthorhombic II-Rh_2O_3 and RhO_2 phases at 500°C, the orthorhombic II-Rh_2O_3 phase at 850°C, and the orthorhombic II- and III-Rh_2O_3 phases at 1000°C. In that study, the support also underwent phase transformation from the γ-alumina phase to its thermodynamically stable α-alumina phase. At 500°C, the dominant phases were γ- and δ-alumina, whereas at 850°C, most of the alumina had transformed to δ- and θ-alumina, and at 1000°C, the dominant phase was α-alumina.

CONCLUSIONS

The distribution of the rhodium oxides formed during the aging of α-alumina supported rhodium in air is affected by epitaxy between the oxide particle and the support. Based on thermodynamics, tetragonal RhO_2 is predicted to be the most stable phase of rhodium oxide at 500°C. The concurrent appearance of hexagonal I-Rh_2O_3 at this temperature is attributed to the stabilization of this phase in epitaxy with the support. Epitaxial stabilization of hexagonal I-Rh_2O_3, rather than the thermodynamically preferred orthorhombic III-Rh_2O_3 phase, is observed when aging occurs at 850°C, as is the appearance of orthorhombic II-Rh_2O_3 when aging occurs at 1000°C. Analysis of the present results demonstrates that epitaxial stabilization of a phase is most pronounced when the rhodium oxide particles are small (<100 Å) and there is a good match between a facet of the oxide particle and one of the exposed facets of the support.

ACKNOWLEDGMENTS

This work was supported by the Office of Chemical Sciences, Division of Basic Energy Sciences, of the U.S. Department of Energy under Contract DE-AC03-76SF00098 at Lawrence Berkeley National Laboratory. Access to the facilities at the National Center for Electron Microscopy is acknowledged. Z. Weng-Sieh gratefully recognizes support through a Noyce Foundation Fellowship.

REFERENCES

1. Taylor, K. C., *Catal. Rev. Sci. Tech.* **35**, 457 (1993).
2. Clean Air Act Amendments, Detailed Summary of Titles, U.S. EPA, Nov. 30, 1990.
3. Yao, H. C., Stepien, H. K., and Gandhi, H. S., *J. Catal.* **61**, 547 (1980); Yao, H. C., Japar, S., and M., Shelef, *J. Catal.* **50** (1977).
4. Beck, D. D., and Carr, C. J., *J. Catal.* **144**, 296 (1993).
5. Beck, D. D., and Carr, C. J., *J. Catal.* **144**, 311 (1993).
6. Weng-Sieh, Z., Gronsky, R., and Bell, A. T, *J. Catal.* **170**, 62 (1997).
7. McCabe, R. W., Usmen, R. K., Ober, K., and Gandhi, H. S., *J. Catal.* **151**, 385 (1995).
8. Yao, H. C., Gandhi, H. S., and Shelef, M., *in* "Metal-Support and Metal-Additive Effects in Catalysis" (B. Imelik *et al*., Eds.), Elsevier, and Amsterdam, 1982.
9. Lakis, R. E., Lyman, C. E., and Stenger, H. G., *J. Catal.* **154**, 261, 276 (1995).

10. Wold, A., Arnott, R. J., and Croft, W. J., *Inorg. Chem.* **2**, 972 (1963).
11. Shannon, R. D., and Prewitt, C. T., *J. Solid State Chem.* **2**, 134 (1970).
12. Biesterbos, J .W. M., and Hornstra, J., *J. Less-Common Met.* **30**, 121 (1973).
13. Lunde, G., *Z. Anorg. Chem.* **163**, 345 (1927).
14. Muller, O., and Roy, R., *J. Less-Common Met.* **16**, 129 (1968).
15. Carol, L. A., and Mann, G. S., *Oxid of Met.* **34**, 1 (1990).
16. Poeppelmeier, K. R., Newsam, J. M., and Brown, J. M., *J. Solid State Chem.* **60**, 68 (1985).
17. Porter, D. A., and Easterling, K. E., "Phase Transformations in Metals and Alloys." VMR International, London, 1981.
18. Zunger, A., and Wood, D. M., *J. Cryst. Growth* **98**, 1 (1989).
19. Rau, C., Schneider, C., Xing, G., and Jamison, K., *Phys. Rev. Lett.* **57**, 3221 (1986).
20. Kolodziejski, L. A., Gunshor, R. L., Otsuka, N., Gu, B. P., Hefetz, Y., and Nurmikko, A. V., *Appl. Phys. Lett.* **48**, 1482 (1986).
21. Sands, T. D., Washburn, J., and Gronsky, R., *Phys. Status Solidi A*, **72**, 304 (1982).